New insight into indium electrochemistry in a Tf2N-based room-temperature ionic liquid

Youssouf Traore, Sophie Legeai, Sébastien Diliberto, Guilhem Arrachart, Stéphane Pellet-Rostaing, Micheline Draye

New Insight into Indium electrochemistry in a Tf_2N – based Room-Temperature Ionic Liquid

Youssouf Traore[a], Sophie Legeai[b,*] , Sébastien Diliberto[a], Guilhem Arrachart[c], Stéphane Pellet-Rostaing[c], Micheline Draye[a*]

[a]*Laboratoire de Chimie Moléculaire et Environnement, Université de Savoie, Campus scientifique, 73376 Le Bourget du Lac Cedex, France*

[b]*Institut Jean Lamour, UMR 7198, Groupe Chimie et Electrochimie des Matériaux, Université Paul Verlaine-Metz, 1 bd Arago, 57078 Metz Cedex 3, France*

[c]*Institut de Chimie Séparative de Marcoule, CNRS/CEA/ENSCM, UMR 5257, Laboratoire Tri ionique par les Systèmes Moléculaires auto-assemblés, Bât. 406, Route de Marcoule, 30207 Bagnols sur Cèze, France*

Y. Traore Youssouf.Traore1@etu.univ-savoie.fr Tel : +33-479-75-88-98 Fax : +33-479-75-86-74

S. Legeai sophie.legeai@univ-metz.fr Tel : +33-387-31-54-63 Fax : +33-387-31-54-60

S. Diliberto sebastien.diliberto@univ-metz.fr Tel : +33-387-31-54-60 Fax : +33-387-31-54-60

G. Arrachart guilhem.arrachart@cea.fr Tel : +33-466-79-15-68 Fax : +33-466-79-76-11

S. Pellet-Rostaing stephane.pellet-rostaing@cea.fr Tel : +33-466-33-93-08 Fax : +33-466-79-76-11

M. Draye micheline.draye@univ-metz.fr Tel : +33-479-75-88-59 Fax : +33-479-75-86-74

Abstract

In this paper we first present the synthesis and the physicochemical properties of low hygroscopic piperidinium-based ionic liquids that allow performing electrodeposition without the need of a glove box. A deep analytical study of the electrochemical system In(III)/In(0) in a 1-butyl-1-ethylpiperidinium bis(trifluoromethylsulfonyl)imide electrolyte ($BEPipTf_2N$) is then described. Troublesome aspects of using chloride metallic precursors in Tf_2N-based electrolytes are highlighted using cyclic votammetry and stripping experiments. Indeed, voltammograms reveal a complex electrochemical behaviour and several cathodic and anodic signals that can be attributed to the formation of indium chlorocomplexes during the scan, due

to changes of concentrations ratio [Cl^-]/[In(III)] of interfacial species during In(III) reduction reaction. In(III)/In(0) electrochemical system and metallic indium electrodeposition in a chloride-free electrolyte is then presented. The use of a chloride-free electrolyte leads to an improvement of electrodeposits morphology and to an increase in faradic yield from 33% to 85%.

Keywords: piperidinium, ionic liquid, indium, electrodeposition

1. Introduction

Indium electrochemical deposition (ECD) is of great interest for the production of thin film semiconducting compounds (InSb, InAs, $Cu(In,Ga)(S,Se)_2$...) that are widely used in electronic and optoelectronic devices (detectors, laser, photovoltaics, light emitting diodes). ECD of indium-containing compounds in aqueous media has been extensively reported in the literature [1,2], pointing out that deposition efficiency is limited by H^+ reduction.

Low melting point ionic liquids or room-temperature ionic liquids (RTILs) are a new class of non aqueous solvents considered as promising electrolytes for ECD of high quality thin films since in this media hydrogen evolution does not occur [3-9]. They are liquid at room-temperature or even below and they are characterized, in particular, by good ionic conductivities and wide electrochemical windows [10]. Two main families of RTILs are commonly used for ECD purposes: halide - based compounds, also called first generation RTILs, and second generation « air and water stable » RTILs. Numerous examples on the use of first generation RTILs for the ECD of single metals and alloys have been reported [11]. However, these chloroaluminate RTILs, combining aluminum chloride and dialkyl-imidazolium or dialkyl-pyridinium chloride, are highly hygroscopic and moisture exposure must be avoided by working in a glove box. The use of RTILs drastically increased since

Wilkes et al. reported in 1992 the first air and moisture stable RTILs, called second generation RTILs, with either tetrafluoroborate or hexafluorophosphate as anions [12]. More recently, RTILs containing anions such as tri-fluoromethanesulfonate, bis(trifluoromethanesulfonyl)imide or tris(trifluoromethanesulfonyl)methide, were synthesized and received much attention because of their low viscosity, low hygroscopy and low reactivity against moisture [13]. However, currently developed and commercialized electrolytes must still be used in dry atmosphere for ECD applications and thus could not be considered as viable electrolytes by electroplating industries.

Moreover, contrary to the common belief, second generation RTILs are not "supersolvents" in which all kinds of materials can be dissolved easily. In fact, due to the poor solvating power of these RTILs composed of weakly coordinating anions, and to their modest polarity, the solubility of inorganic ionic compounds in second generation RTILs is very low excepted using chloride salts. However, the introduction of chloride ions in electroplating baths leads to undesirable chlorine gas evolution at the anode during ECD, increases hygroscopic character of the RTIL and leads in some cases to complex electrochemical behaviors.

ECD of In has been recently studied in an air and moisture stable RTIL, using a chloride salt as indium cation source [14]. In these conditions, In(III)/In(0) electrochemical system is far from simple, implying several reduction steps that are difficult to explain and lead to complex optimisation of ECD experimental parameters for high quality films synthesis. Moreover, in this previous work, experiments were carried out in highly restrictive conditions, namely in a glove box with water and oxygen concentration levels below 1 ppm. Indeed, the electrolytic solutions used, consisting in a 1-butyl-1-methylpyrrolidinium bis(trifluoromethylsulfonyl)imide ($BMPTf_2N$) RTIL containing $InCl_3$ as metallic precursor, is too hygroscopic to perform ECD experiments in ambient atmosphere.

In this paper, we first relate the synthesis and some physico-chemical properties of new low hygroscopic piperidinium - based RTILs. We then present a detailed study of the electrochemical behavior of $InCl_3$ in the most convenient RTIL for In(0) ECD, 1-butyl-1-ethyl-piperidinium bis(trifluoromethylsulfonyl)imide ($BEPipTf_2N$). The strong influence of Cl^- ions on In(III)/In(0) electrochemical system is highlighted. Finally, some results concerning In(0) ECD using an indium soluble anode as In(III) precursor are compared to those obtained with an $InCl_3$ – containing RTIL.

2. Experimental

Ionic liquids were prepared according to the procedure modified from the published report of A. Triolo et al. [15]. Briefly, nitrogen based heterocycle yielded the corresponding ammonium salt by reaction with alkyle bromide. Bromide anion was then replaced by bis(trifluoromethylsulfonyl)imide (Tf_2N^-) by vigorous stirring of the alkylammonium bromide with aqueous solution of lithium bis(trifluoromethylsulfonyl)imide ($LiTf_2N$, Solvionic, 99+%). After metathesis was finished ionic liquid was extracted with dichloromethane (Sigma Aldrich, >99.5%) and then dried under reduced pressure for 3 hours. Synthesized ionic liquids were characterized by Nuclear Magnetic Resonance (NMR) analysis (Bruker Spectrospin DRX 300 MHz Ultrashield).

The density, the viscosity and the conductivity of RTILs were determined as function of water content which was determined by Karl Fischer coulometric titration (Metrohm 831KF coulometer) using Hydranal 34843 Coulomat AG-H (Fluka) as titrant.

The density measurements were performed with a thermo-regulated digital densimeter DSA 5000 (Anton Paar). The apparatus measures densities using an oscillating U-tube at an accuracy of 0.00001g/cm^3 and temperature controlled with an accuracy of 0.001°C.

All measurements were conducted at 20.005±0.004°C; the density is calculated from the quotient of the period of oscillations of the U-tube and the reference oscillator: density = KA x Q^2 x f_1 – KB + f2, where KA, KB are constants from the apparatus, Q the quotient of the period of oscillation of the U-tube divided by the period of oscillation of the reference oscillator and f_1, f_2 correction terms for temperature, viscosity and nonlinearity.

All rheological measurements were performed on an automated microviscosimeter AMVn (Anton Paar). The apparatus measures viscosities in a 0.3 – 2500mPa.s range using the rolling ball/falling ball principle which consist of the measurement of a ball rolling time in a diagonally mounted glass capillary filled with the sample. Ball rolling time was measured at an accuracy of 0.002 sec with a temperature controlled with an accuracy of 0.001 C.

All measurements were conducted at 20.00°C with a 70° inclination angle of the capillary, the dynamic viscosity η is calculated using the following formula $\eta = K_1 \times (\rho_K - \rho_P) \times t_1$ where K_1 is the calibration constant of the measuring system, ρ_K the ball density, ρ_P the density of the measured sample and t_1 the ball rolling time.

Conductivities of RTILs were measured using a Tacussel électronique conductimeter/resistivitimeter CDRV62 using a platinum 2-electrodes cell (Materials Mates). The cell was calibrated with 5×10^{-3} to 3.3×10^{-2} KCl solutions and the data were recorded at a frequency of 62 Hz.

The solubility of water in the RTILs was determined by Karl Fischer coulometric titration after RTILs contact with distilled water. The water content of water-saturated RTILs in equilibrium with water was measured by mixing water and each RTIL for 24 h. After that, the two-phase system was centrifuged and RTIL water content was measured.

Electrochemical experiments were carried out using a PGP201 potentiostat (Radiometer Copenhagen) and a Tacussel Electronique potentiostat (101T and PJT24-1). Before electrochemical experiments, the electrolytic solution was deaerated and dried down to water

contents below 50 ppm by dry Ar bubbling. In(III) solutions were prepared whether by dissolution of $InCl_3.4H_2O$ (Sigma Aldrich, 97%) or by electrochemical potentiostatic dissolution of an indium soluble anode (Alfa Aesar, 99.99%) in the selected ionic liquid at ambient temperature. All experiments were performed at 60°C to lower RTILs viscosity and increase mass transport. Electroanalytical studies were carried out using a conventional three-electrode electrochemical cell, with a platinum disk (19.6 mm^2) as working electrode, a glassy carbon as counter electrode and an AgCl-covered Ag wire (Alfa Aesar 99,999%) as pseudo-reference electrode. Square plates of Pt (Goodfellow, Lille, France, 99.99%, area 25.0 mm^2) were used as substrates for the electrodeposition of indium. Electrodeposition was achieved by controlled potential electrolysis in steadily stirred $BEPipTf_2N$ containing In(III). Before the electrochemical experiments were carried out, the working electrode was polished with SiC abrasive papers and 1 µm diamond paste, and then soaked in deionized water and acetone. After electrodeposition, the indium-coated Pt-square plate electrodes were immediately transferred from the electrodepositing baths into acetone to remove the residual RTIL.

The surface morphology and grain size of the deposits were determined using a scanning electron microscope (FEG-SEM) (Philips XL30), provided with an energy dispersive spectrometry (EDS) detector. Structural characterizations were conducted by X-ray diffraction (XRD) using a Bruker diffractometer (D8 Advance, Cu $K\alpha_1$ radiation).

ECD faradic yields were determined by Atomic Absorption Spectrometry (Varian AA240FS) after chemical dissolution of the deposits in 3M HNO_3.

3. Results and Discussion

3.1. Physicochemical properties of 1,1-dialkyl-$PipTf_2N$ RTILs

Few literature reports deal with piperidinium-based RTILs because of their little commercial availability [16][1]. However, their physicochemical properties can be compared to more extensively used pyrrolidinium- and imidazolium-based RTILs [10,16-21].

The density, electrochemical stability, conductivity and viscosity of several 1,1-dialkyl-PipTf_2N RTILs as well as the solubility of water in these solvents are presented in Table 1 and compared to results obtained with imidazolium and pyrrolidinium-based RTILs (our results and literature data). As the density, the conductivity and the viscosity of ionic liquids can be affected by water impurities, values are reported in Table 1 along with corresponding RTIL water content in italics.

Table 1: RTILs physicochemical properties

Physicochemical properties determined in this work are in good agreement with literature data, when available. Results obtained for cathodic stability cannot be compared to literature data as these latter refer to other reference electrode devices. Cathodic stability and water solubility values obtained in this work follow the order BMITf_2N < BMPyrrolTf_2N ~ BMPipTf_2N ~ BEPipTf_2N ~ MOPipTf_2N~ < EOPipTf_2N. It appears then that all piperidinium-based RTILs tested present a wider electrochemical window and a lower hygroscopic character than other RTILs under consideration. It is commonly admitted that RTILs based on saturated-ring cations, like pyrrolidinium or piperidinium cations, present higher cathodic stability than unsaturated-ring cations, like imidazolium or pyridinium-based cations as well as octyl-substituted cations compared to butyl-substituted cations [10]. However, piperidium ring lead to more viscous and consequently less conductive RTILs

compared to imidazolium or pyrrolidinium similar compounds. Finally, increasing cations alkyl chain length also leads to a decrease in conductivity of RTILs mainly due to an increase in viscosity, as commonly observed [10].

The best compromise between cathodic stability, conductivity and hygroscopic character appears to be $BEPipTf_2N$, and this RTIL was selected for the further studies. According to Table 1, $BEPipTf_2N$ appears to be hygrophobic enough to work without the need of a glove box.

3.2. Electrochemical behavior of $InCl_3$ - containing electrolytes

Figure 1 shows a typical cyclic voltammogram on Pt working electrode in $BEPipTf_2N$ containing 0.1 M $InCl_3$. It appears that the cyclic voltammogram is quite complex: several cathodic ($c_1 – c_5$) and anodic ($a_1 – a_5$) processes can be observed in the whole potential range tested. In order to elucidate the complete voltammogram, several experiments were undertaken by cyclic voltammetry and potentiostatic deposition followed either by anodic stripping or by XRD/SEM-EDS analysis of corresponding deposits.

Figure 1: Cyclic voltammograms recorded on platinum in $BEPipTf_2N$.Scan rate 5 mV/s. T =60°C.

3.2.1. Electrodeposition of In on Pt square plates and surface analysis of potentiostatic deposits

1 hour potentiostatic deposition experiments were realised for several potential values, corresponding to c_1 – c_5 peaks on platinum square electrodes. XRD patterns confirm the presence of metallic In for potential values lower than 200 mV vs AgCl/Ag. Figure 2 shows a typical XRD pattern of In(0) deposits obtained at E_{dep} = -920 mV vs AgCl/Ag.

Figure 2: XRD pattern of an indium deposit on a platinum substrate. $BEPipTf_2N$ + $InCl_3$ 0.1 M. E_{dep} = -920 mV vs AgCl/Ag, t_{dep} = 1h. T =60°C.

SEM-EDS analysis revealed that c_1, c_2 and c_4 applied potentials only lead to low amounts of In(0) on the electrode and that only c_5 peak corresponds to bulk deposition. This result was already observed by S. Zein el Abedin et al. [14], who supposed that c_1 to c_4 peaks may correspond to multiple UPD/Pt-alloying processes, but this hypothesis was neither confirmed nor denied by detailed experimental electrochemical investigations. Moreover, the absence of metallic indium deposition between c_3 and c_4 is quite surprising. This behavior is drastically different from what was previously published. Indeed, very simple voltammetric curves with only single electrochemical signals were recorded using other substrates (Mo [22,23], glassy carbon [24-26], Hg [1,27] , In [1,28]) and other solvents (high temperature molten salts [23,24,28], RTILs [22, 25] or aqueous medium [1,27].

3.2.2. Detailed voltammetric study of In(III) in $BEPipTf_2N$

In order to get a deeper understanding of In(III)/In(0) electrochemical system in our electrolyte, a detailed voltammetric study was undertaken. First of all, to identify possible alloying processes with Pt substrate, the voltammogram obtained on Pt was compared to a cyclic voltammogram performed using a stainless steel working electrode (Figure 3). Using stainless steel, anodic potential windows is limited by electrode oxidation and consequently, a_1 and a_2 peaks could not be studied.

Figure 3: Cyclic voltammograms recorded in $BEPipTf_2N$ containing 0.1 M $InCl_3$ on platinum and stainless steel. Scan rate 5 mV/s. T =60°C.

Cyclic voltammograms present roughly the same characteristics using both electrodes, except c_1 signal which is not observed on steel. According to this observation, only c_1 signal recorded on platinum substrate might be attributed to an In-Pt alloying process.

Voltammetric experiments by varying cathodic reversal potentials were then carried out using the Pt electrode, in order to study the other electrochemical signals (Figure 4b-e). The complete voltammogram is reminded as Figure 4a.

Figure 4: Cyclic voltammograms recorded on platinum in $BEPipTf_2N$ containing 0.1 M $InCl_3$ with different reversal potentials. Scan rate 5 mV/s. T =60°C.

When the scan is reversed just after peak c_1 at +50 mV vs AgCl/Ag (Figure 4e), two oxidation peaks, a_1 and a_2, are observed during the return scan. According to previous results (Figure 2), these anodic peaks might result from an In-Pt alloying process occurring at c_1.

Decreasing cathodic potentials down to -100 mV vs AgCl/Ag, a new anodic peak a_3 appears during the reverse scan, which intensity increases when decreasing reversal potential (Fig 4e). The electrochemical signal c_2 can then be attributed to the deposition of metallic indium. Complementary potentiostatic experiments were undertaken at -100 mV vs AgCl/Ag for several deposition times, followed by anodic stripping using linear voltammetry (Figure 5a). The results obtained confirmed the hypothesis of c_2 corresponding to In(0) deposition and a_3 corresponding to elemental In stripping.

Surprisingly, by further decreasing the reversal potential down to -500 mV vs AgCl/Ag, the intensity of a_3 anodic peak decreases (Figure 4d). Simultaneously, a_1 increases with potential switching getting more cathodic. Potentiostatic deposition at c_3 peak potential followed by anodic stripping was also performed for several deposition times. The results obtained confirm the decrease of a_3 anodic peak and the increase of a_1 with increasing deposition time (Figure 5b). One can also notice the shape of c_3 peak, characteristic of a surface reaction limited by a finite amount of matter, that suggests that In(0) previously deposited might undergo an electrochemical transformation (surface rearrangement, second In-Pt alloying step…). At this date, none of experiments performed allow us to make any hypothesis concerning the electrochemical reaction corresponding to c_3 cathodic peak.

Figure 5: Voltammograms recorded during anodic stripping of indium in $BEPipTf_2N$ containing 0.1 M $InCl_3$, for different deposition charge values. Platinum substrate. Scan rate 5 mV/s. T = 60°C.

a: E_{dep} = -100 mV vs AgCl/Ag

b: E_{dep} = -200 mV vs AgCl/Ag

According to Figure 4b and 4c, c_5 cathodic peak that was previously attributed to bulk deposition of In(0) thanks to XRD analysis, is related to three anodic stripping peaks: a_3, a_4 and a_5. The link between c_5 and a_3 is in agreement with previous observations attributing a_3 signal to In(0) stripping (Figure 4e). As shown on Figure 4b, a_3 peak is only observed for switching potential lower than -920 mV vs AgCl/Ag and its peak current then increases with switching potential getting more cathodic. Conversely, a_4 and a_5 peak currents reach constant values for potentials lower than -1200 mV vs AgCl/Ag.

In order to confirm voltammetric results, potentiostatic experiments were undertaken at c_5 peak potential for increasing deposition times, followed by anodic stripping using linear voltammetry. Results obtained are presented in Figure 6a.

Figure 6a: Voltammograms recorded during anodic stripping of indium in $BEPipTf_2N$ containing 0.1 M $InCl_3$, for different deposition charge values. Platinum substrate. Scan rate 5 mV/s. T = 60°C. E_{dep} = -920 mV vs AgCl/Ag.

As can be observed, only a_3 peak grows significantly with deposition time meaning that a_3 signal can be related to the anodic "bulk" dissolution of In(0) previously deposited. Figure 6b presents anodic charges Qa_3, Qa_4 and Qa_5, corresponding respectively to peaks a_3, a_4 and a_5, as well as $Q_{a\ total} = Qa_3 + Qa_4 + Qa_5$, as a function of cathodic charge Q_c related to potentiostatic deposition.

Figure 6b: Anodic charges corresponding to potentiodynamic stripping of indium *(voltammograms presented in Fig. 6a)* as a function of cathodic charge related to potentiostatic deposition. BEPipTf$_2$N containing 0.1 M $InCl_3$.Platinum substrate. T = 60°C. E_{dep} = -920 mV vs AgCl/Ag.

$Q_{a\ total}$ grows linearly with Q_c, meaning that the three anodic peaks under consideration can be related to anodic dissolution of In(0) deposited during the potentiostatic step. Considering separately anodic charges Qa_3, Qa_4 and Qa_5, one can observe that Qa_3 increases linearly with Q_c for deposition times longer than 2 min, whether Qa_4 and Qa_5 remains constant in the same range of deposition time. On the other hand, for deposition times shorter than 2 minutes, the inverse behavior is observed: Qa_4 and Qa_5 increase linearly with Q_c, whereas Qa_3 only slowly increases (see inset Figure 6b). It appears then that a_5 and a_4 signals might be related to mass transport limited processes associated with metallic indium dissolution. An hypothesis that can be made is that a_4 and a_5 signals could be related to the formation of species limited by chloride ions mass transport, like $In_xCl_y^{3x-y}$ complexes. Indeed, these electrochemical processes cannot be observed when using chloride-based RTILs [22,25] or high temperature molten salts [23,24,28] in which chloride mass transport is not limiting, as chloride ions are

not present as solutes but as part of the solvent. It must be kept in mind that RTIL are viscous media in which mass transport is very slow. The hypothesis of a limitation by chloride ions mass transport is also comforted by the diffusional shape of a_5 signal. The same hypothesis could also explain that c_2 and c_5 cathodic signals are both related to In(0) deposition and could correspond to the reduction of several In(III) - based species.

3.3. Influence of chloride ions on In(III)/In(0) electrochemical behavior

3.3.1. In(III) electrochemical behavior in a chloride-free electrolyte

In order to validate the previous hypothesis concerning the influence of Cl^- ions on In(III) electrochemical behavior, a chloride-free electrolytic solution was studied. In(III) ions were introduced in the RTIL by potentiostatic oxidation of an In soluble anode. The counter electrode was isolated in a salt bridge to avoid electrolyte degradation. The concentration of In(III) species was calculated by the mass loss of the soluble anode. A typical cyclic voltammogram of the resulting solution is given in Figure 7.

Figure 7: Cyclic voltammogram of a 1.87 x 10^{-2} M In(III) solution of chloride-free BEPipTf_2N. Scan rate 5 mV/s. T =60°C. Pt substrate.

A very simple voltammogram is obtained compared to those previously recorded using $InCl_3$. A single electrochemical system is observed, with a nucleation loop at -70 mV vs AgCl/Ag, characteristic of a metallic deposition process. This voltammogram is very similar to the one obtained using $InCl_3$ in chloride-based electrolytes [22-25,28] and is characteristic

of a single species in solution. In chloride-based RTIL, In(III) exists solely as $In_2Cl_5^{2-}$. In our case, In(III) may exist as In^{3+} or $In_x(Tf_2N)_y^{3x-y}$.

XRD/SEM-EDS analysis of potentiostatic deposits confirmed the presence of metallic In for deposition potential values lower than -80 mV vs AgCl/Ag.

3.3.2. Influence of Cl^- concentration on the electrochemical behavior of In(III) in $BEPipTf_2N$

The influence of Cl^- concentration on the electrochemical behavior of In(III) was studied by adding increasing amount of a chloride-based RTIL in the previously prepared chloride-free In(III) solution. Figures 8a-d presents the corresponding voltammograms recorded at the Pt electrode.

Figure 8: Cyclic voltammograms of a 1.87 x 10^{-2} M In(III)-containing $BEPipTf_2N$ solution, recorded for different values of the $[Cl^-]/[In(III)]$ ratio. Scan rate 5 mV/s. T =60°C. Pt substrate.

As can be observed, as soon as Cl^- ions are introduced in the In(III) solution, a second electrochemical system appears, characterized by a cathodic peak at -850 mV vs AgCl/Ag and a corresponding anodic peak at -800 mV vs AgCl/Ag (Figure 8a). This electrochemical system progressively shifts towards more cathodic potential values as Cl^- concentration increases (Figure 8b-c). Corresponding peak currents increase with Cl^- concentration and one can observe the simultaneous decrease of peak currents related to "free"-In(III)/In(0) system. This behavior reveals the presence of indium chloride species $In_xCl_y^{3x-y}$. By overlaying the cyclic voltammogram recorded in a $InCl_3$ - containing electrolyte of identical In(III) concentration, it appears that the electrochemical signals c_5/a_5 correspond to an $In_xCl_y^{3x-}$

^{y}/In(0) electrochemical system (Figure 8d). One can also conclude from these experiments that the electrochemical signals c_2/a_3 correspond to the “free” In(III)/ In(0) system. The exact formula of the chloride complex could not be determined as cyclic voltammograms are affected by the progressive increase of electrolyte viscosity with chloride-based RTIL addition. This could also explain that the voltammogram recorded for a $[Cl^-]/[In(III)]$ ratio of 3 does not match, in terms of peak intensities, with the voltammogramm corresponding to the $InCl_3$ - containing electrolyte.

These experiments highlight the formation of indium-chloride complex species during the running of a cyclic voltammetry experiment. This phenomenon can be explained by the changes in interfacial relative concentrations of In(III) and Cl^- species during the cathodic/anodic scans, due to In(III) consumption/formation. When the cathodic scan progresses, In(0) deposition occurs and the interfacial ratio $[Cl^-]/[In(III)]$ increases leading to the formation of $In_xCl_y^{3x-y}$ species that are reduced at more cathodic potentials. At the beginning of the forward scan, the ratio $[Cl^-]/[In(III)]$ is high and the stripping of In(0) previously deposited leads first to the formation of an indium-chloride complex. The interfacial ratio $[Cl^-]/[In(III)]$ then decreases and In(0) stripping reaction leads to the formation of “free”-In(III). This hypothesis is confirmed by deposition/stripping experiments (Figure 6): as the amount of deposited In(0) increases, a_5 peak reaches a constant value related to the limiting mass transport of Cl^- species, whereas a_3 peak increases.

These multiple electrochemical processes are due to the use of a Tf_2N-based electrolyte associated to a chloride-based metallic precursor. The same electrochemical behavior could be observed with any metallic ion that may form complex species with the counter-anion of its metallic precursor salt. It has already been observed for $SeCl_4$-containing RTILs: a single

electrochemical system was observed by Dale et al. [22] in a chloride-based RTIL whereas Zein el Abedin et al. [14] recorded a very complex voltammogram in a Tf_2N -based RTIL.

More experiments would be necessary to completely understand the electrochemical behavior of $InCl_3$ containing Tf_2N-based RTIL, as some electrochemical signals cannot obviously be explained by the presence of chloride ions.

3.4. Electrochemical deposition of In

Indium electrodeposition was performed under potentiostatic conditions using both $InCl_3$ - containing electrolytes and chloride-free electrolytes containing In(III) species introduced by anodic dissolution of an In anode. Using $InCl_3$ - containing RTILs, deposition experiments were only conducted in the potential range corresponding to the bulk deposition of In(0) (around c_5 signal). In both cases, the following deposition potential values were tested: $E_{1/2}$, E_{peak} and (E_{peak} + 100 mV). Each deposit was analyzed by XRD and SEM-EDS. The faradic yield of each electrodeposition process was evaluated by AAS after chemical dissolution of the deposit in HNO_3 3M.

Adherent, homogeneous and covering deposits were obtained for all experimental conditions tested (Figure 9).

Figure 9: Typical SEM micrographs of indium deposits obtained in $BEPipTf_2N$. Pt substrate. 60 minutes deposition.

a: $BEPipTf_2N$ + $InCl_3$ 9.22 x 10^{-2} M. E_{dep} = -920 mV vs AgCl/Ag.

b: Chloride-free $BEPipTf_2N$. E_{dep} = -140 mV vs AgCl/Ag. [In(III)] = 7.31 x 10^{-2} M.

For each deposit, XRD analysis confirmed the presence of metallic In on the platinum substrate. Average faradic yields obtained for each applied potential are presented in Table 2.

Table 2: Electrodeposition of indium on platinum in BEPipTf$_2$N: average faradic yields.

The highest faradic yields were obtained in both electrolytes for E_{peak} deposition potential. One can notice in Table 2 that faradic yields obtained using the chloride-free electrolyte are much higher than those obtained with the $InCl_3$ – containing solution whatever the deposition potential that was applied. This phenomenon can then be attributed to the presence of Cl^- ions in the electrolyte. These low faradic yields could be related to a secondary electrochemical reaction, the non elucidated cathodic process occurring between c_3 and c_4, that lead to a consumption of metallic indium simultaneously with its bulk deposition.

Besides, the changes in the interfacial ratio [Cl^-]/[In(III)] during deposition process, that leads to the shift of the In(0) deposition potential towards more cathodic values as the ratio [Cl^-]/[In(III)] increases (Figure 8), could explain the improved morphology that was obtained in chloride-free electrolytes compared to $InCl_3$ – containing solutions (Figure 9).

Finally, EDS spectra (Figure 10) reveal the presence of Cl on the deposits realised in $InCl_3$ – containing RTILs, that could be due to chloride ions adsorption on the electrode surface, to the inclusion of chloride ions in the deposits during electrodeposition process or to the formation of chloride indium species, as showed by Carpenter et al. [29]. These species could

also be involved in non identified electrochemical signals on the cyclic voltammogram of $InCl_3$ – containing electrolytes (Figure 1).

Figure 10: EDS analysis of indium deposits obtained in $BEPipTf_2N$.Pt substrate. 60 minutes deposition. *(Sample presented on Figure 9).*

a: $BEPipTf_2N$ + $InCl_3$ 9.22 x 10^{-2} M. E_{dep} = -920 mV vs AgCl/Ag.

b: Chloride-free $BEPipTf_2N$. E_{dep} = -140 mV vs AgCl/Ag. [In(III)] = 7.31 x 10^{-2} M.

4. Conclusion

In the first part of this paper, we presented the synthesis and some physicochemical properties of a new low hygroscopic RTIL, 1-butyl-1ethylpiperidinium bis(trifluoromethylsulfonyl)imide ($BEPipTf_2N$), that allowed us to perform In(0) ECD without the need of a glove box.

The analytical study of the second part reveals the strong influence of Cl^- ions on the electrochemical behavior of In(III). The formation of indium chloride complexes due to the changes of concentrations ratio $[Cl^-]/[In(III)]$ of interfacial species during In(III) reduction reaction is highlighted. The formation of these multiple In-based species results in very complex voltammograms and to a real difficulty to optimize ECD experimental conditions. Another consequence, which is presented in the third part of this paper, is the important decrease of the faradic yield corresponding to In(III) ECD in the presence of Cl^- ions. EDS analysis also reveals the presence of chlorine that may be whether included in the deposits or correspond to non metallic In-based compounds.

This study shows that one must be very careful when using chloride metallic salts in Tf_2N – based RTIL, especially for metallic ions that form stable chloride complexes, for example In(III), Se(IV), Te(IV) or Ga(III). These RTIL are very popular among electrochemists' community because of their low viscosity, their high electrochemical stability and their low hygroscopic character. However, the use of a Tf_2N-based electrolyte associated to a chloride-based metallic precursor can lead to complex electrochemical systems and consequently be prejudicial to ECD processes.

Acknowledgements

The authors gratefully acknowledge the 'Cluster Chimie' of the 'Région Rhône-Alpes' and the GNR CNRS SPDC2 for their financial supports.

References

[1] R. Piercy, N.A. Hampson, J. Appl. Electrochem. 5 (1975) 15

[2] S. Taunier, J. Sicx-Kurdi, P.P. Grand, A. Chomont, O. Ramdani, L. Parissi, P. Panheleux, N. Naghavi, C. Hubert, M. Ben-Farah, J.P. Fauvarque, J. Connolly, O. Roussel, P. Mogensen, E. Mahe, J.F. Guillemoles, D. Lincot, O. Kerrec, Thin Solid Films 480 (2005) 526

[3] Q. Liao, W.R. Pitner, G. Stewart, C.L. Hussey, G.R. Stafford, J. Electrochem. Soc. 144 (1997) 936

[4] E. G.-S. Jeng, I.W. Sun, J. Electrochem. Soc. 144 (1997) 2369

[5] S.-I. Hsiu, I.W. Sun, J. Appl. Electrochem. 34 (2004) 1057

[6] Y. Katayama, S. Dan, T. Miura, T. Kishi, J. Electrochem. Soc. 148 (2001) C102

[7] T.Tsuda, T. Nohira, Y. Ito, Electrochim. Acta 46 (2001) 1891

[8] E.R. Schreiter, J.E. Stevens, M.F. Ortwerth, R.G. Freema, Inorg. Chem., 38 (1999) 3935

[9] W.R. Pitner, C.L. Hussey, J. Electrochem. Soc. 144 (1997) 3095

[10] J.L. Anthony, J.F. Bennecke, J.D. Holbrey, E.J. Maginn, R.A. Mantz, R.D. Rogers, P.C. Trulove, A.E. Visser, T. Welton, in: P. Wasserscheid and T. Welton (Ed.), Ionic Liquids in Synthesis, Wiley-VCH Verlag GmbH & Co., 2002, Ch. 3

[11] G.R. Stafford and C.L. Hussey, in: R.C. Alkire and D.M. Kolb (Ed.), Advances in Electrochemical Science and Engineering, Vol. 7, Wiley-VCH, Weinheim, 2001, Ch. 6

[12] T.L. Riechel, J.S. Wilkes, J. Electrochem. Soc. 139 (1992) 977

[13] M. Gazlinski, A. Lewandowski, I. Stepniak, Electrochim. Acta 51 (2006) 5567

[14] S. Zein el Abedin, A.Y. Saad, H.K. Farag, N. Borisenko, Q.X. Liu, F. Endres, Electrochim. Acta 52 (2007) 2746

[15] A. Triolo, O. Russina, B. Fazio, G. Battista Appetecchi, M. Carewska, and S. Passerini, J. Chem. Phys. 130 (2009) 164521

[16] Z.B. Zhou, H. Matsumoto, K. Tatsumi, Chem. Eur. J. 12 (2006) 2196

[17] I. Mukhopadhyay, C.L. Aravinda, D. Borissov, W. Freyland, Electrochim. Acta 50 (2005) 1275

[18] P. Hapiot, C. Lagrost, Chem. Rev. 108 (2008) 2238

[19] H. Ohno, in: F. Endres, A.P. Abbott and D.R. MacFarlane (Ed.), Electrodeposition from Ionic Liquids, Wiley-VCH Verlag GmbH & Co., 2008, Ch. 3

[20] S. Zein El Abedin, N. Boressinko, F. Endres, Electrochem. Comm. 6 (2004) 510

[21] J. Salminen, N. Papaiconomou, R.A. Kumar, J.M. Lee, J. Kerr, J. Newman, J.M. Prausnitz, Fluid Phase Equilib. 261 (2007) 421

[22] D.D. Shivagan, P. J. Dale, A.P. Samantilleke, L.M. Peter, Thin Solid Films 515 (2007) 5899

[23] Y. Castrillejo, M.R. Bermejo, A.M. Martinez, C. Abejon, J. Appl. Electrochem. 29 (1999) 65

[24] M. Mohamedi, S. Martinet, J. Bouteillon, J.C. Poignet, Electrochim. Acta 44 (1998) 797

[25] M.-H. Yang, M.-C. Yang, I.-W. Sun, J. Electrochem. Soc. 150 (2003) C544[26] J.S.-Y. Liu, I.W. Sun, J. Electrochem. Soc. 144 (1997) 140

[27] R.E. Visco, J. Electrochem. Soc. 112 (1965) 932

[28] M. Mohamedi, J. Bouteillon, J.C. Poignet, Electrochim. Acta 41 (1996) 1495

[29] M.K. Carpenter, M.W. Verbrugge, J. Mater. Res. 9 (1994) 2584

Figures

Figure 1

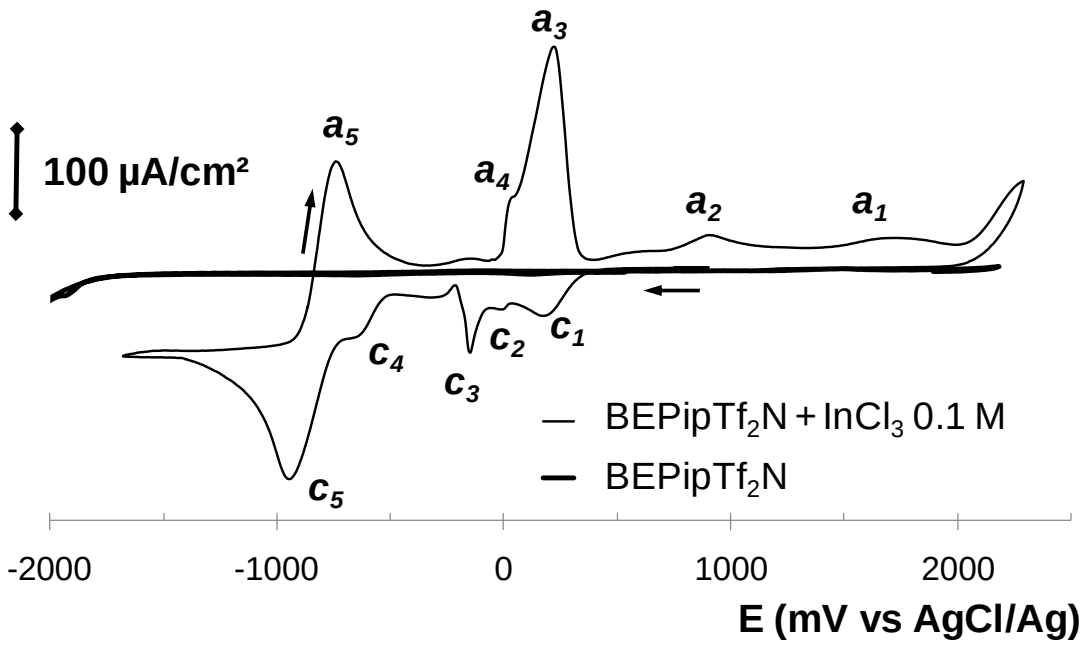

Figure 2

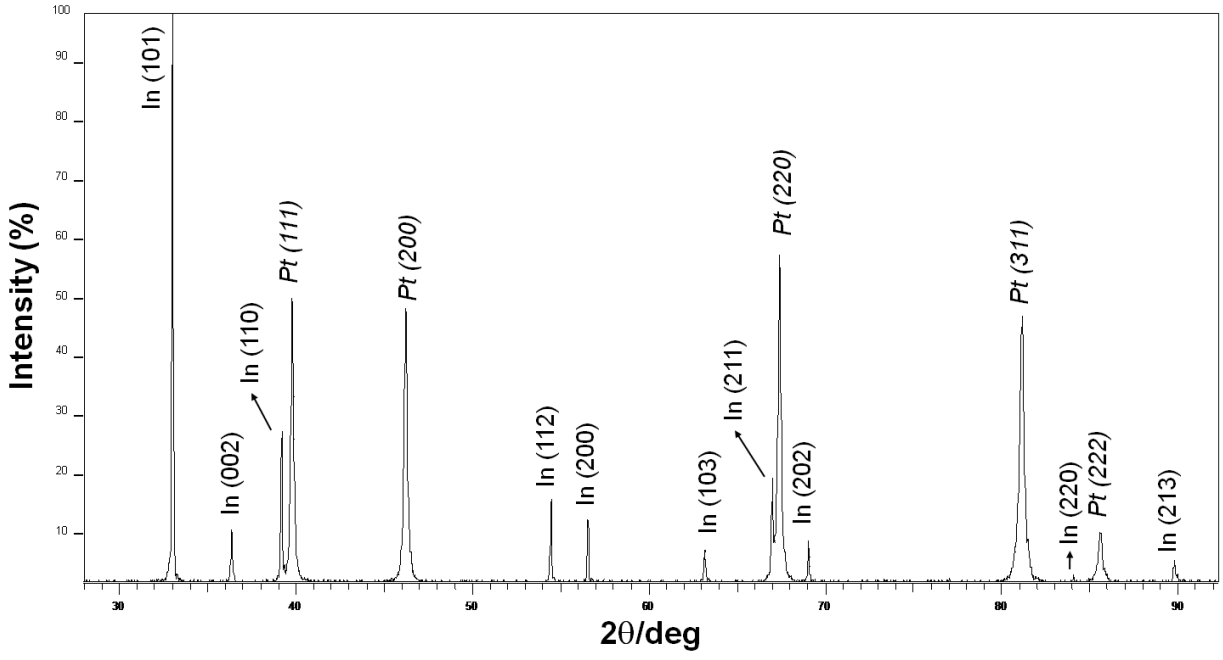

Figure 3

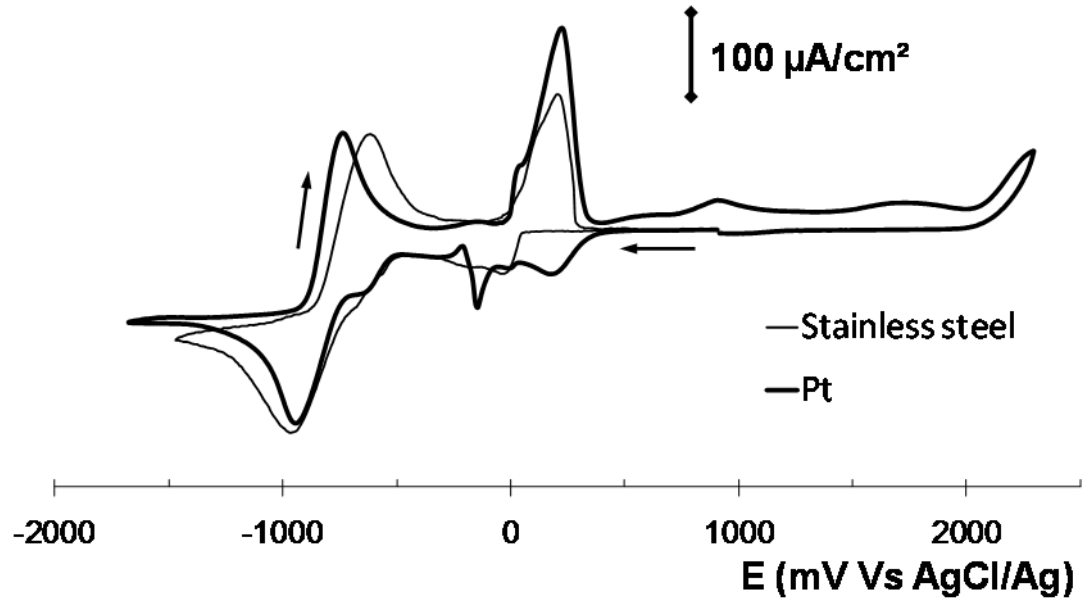

Figure 4

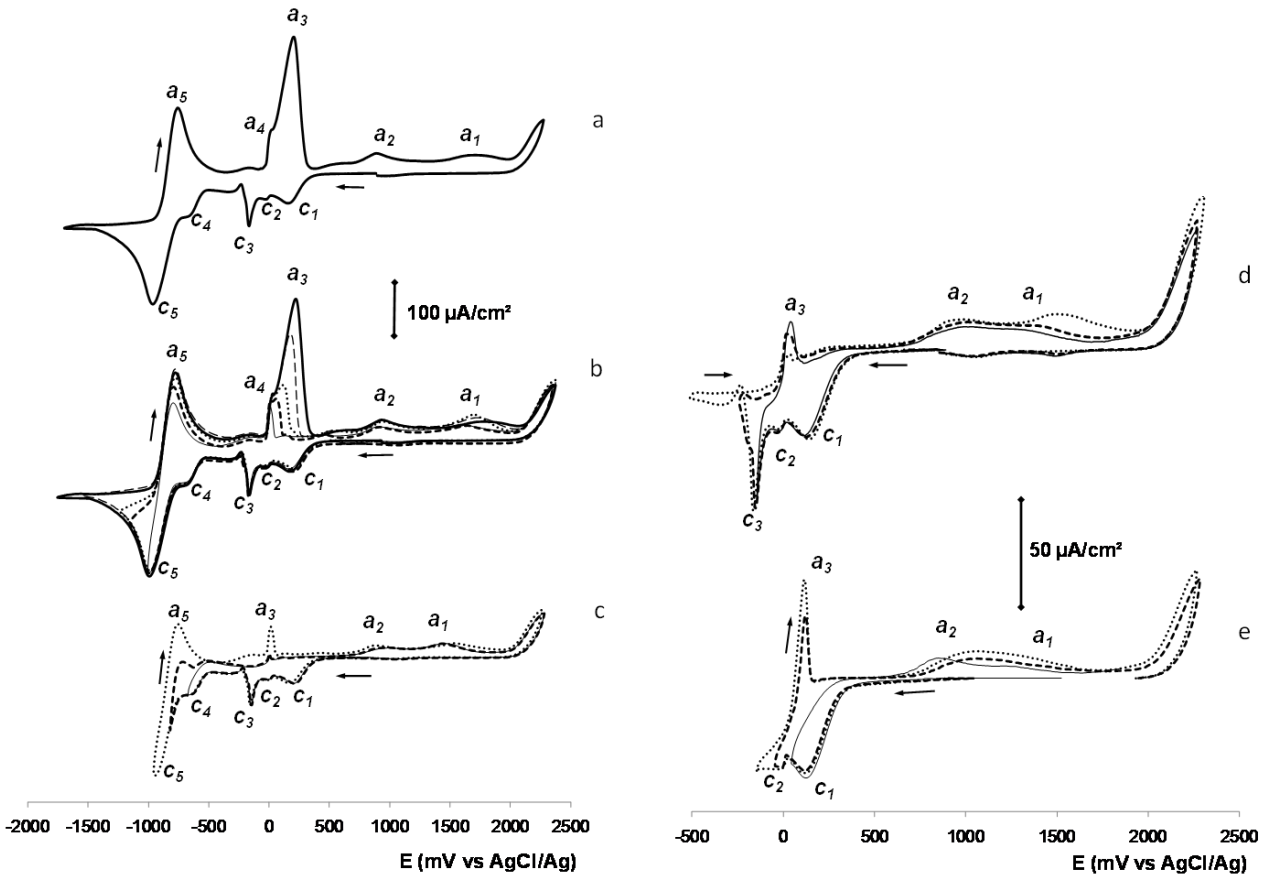

Figure 5

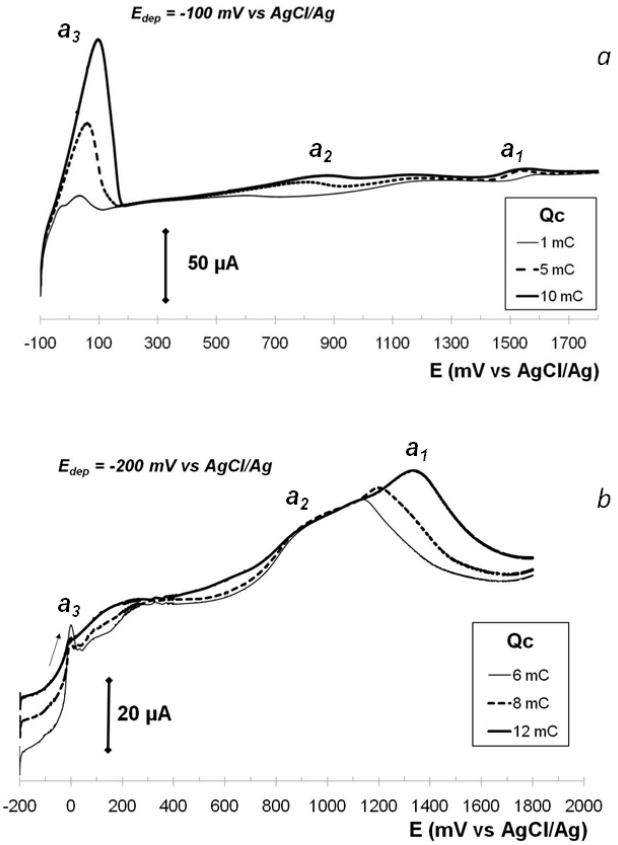
E_{dep} = -100 mV vs AgCl/Ag
a_3
a_2
a_1
a
Qc
1 mC
5 mC
10 mC
50 µA
-100 100 300 500 700 900 1100 1300 1500 1700
E (mV vs AgCl/Ag)
E_{dep} = -200 mV vs AgCl/Ag
a_1
a_2
a_3
b
Qc
6 mC
8 mC
12 mC
20 µA
-200 0 200 400 600 800 1000 1200 1400 1600 1800 2000
E (mV vs AgCl/Ag)

Figure 6a

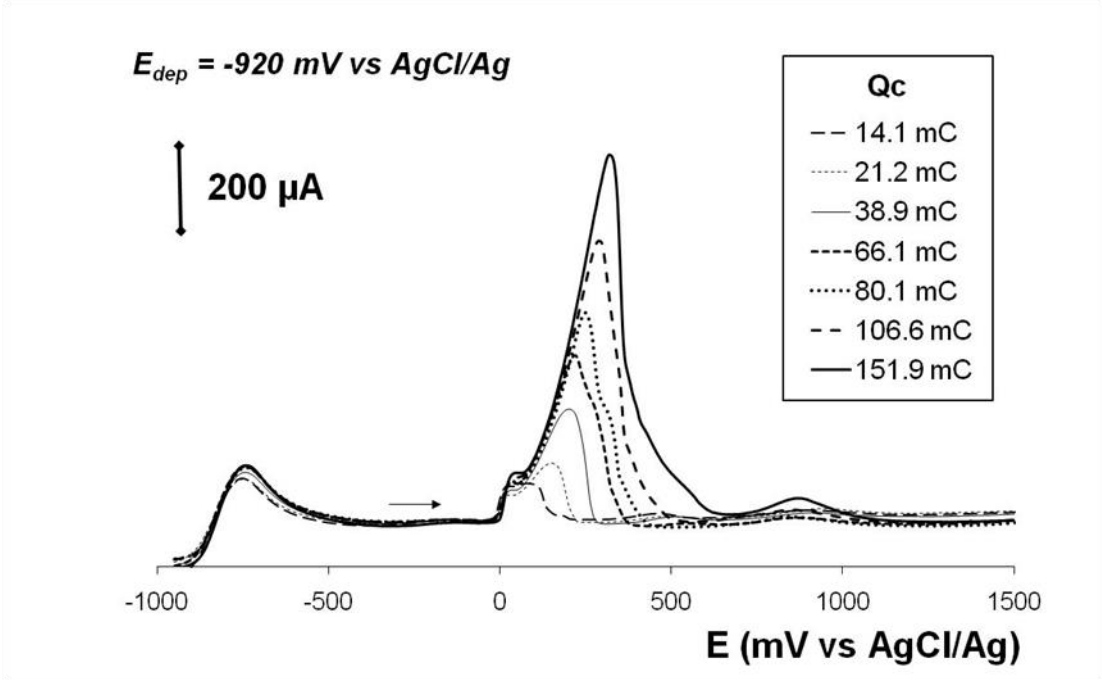

Figure 6b

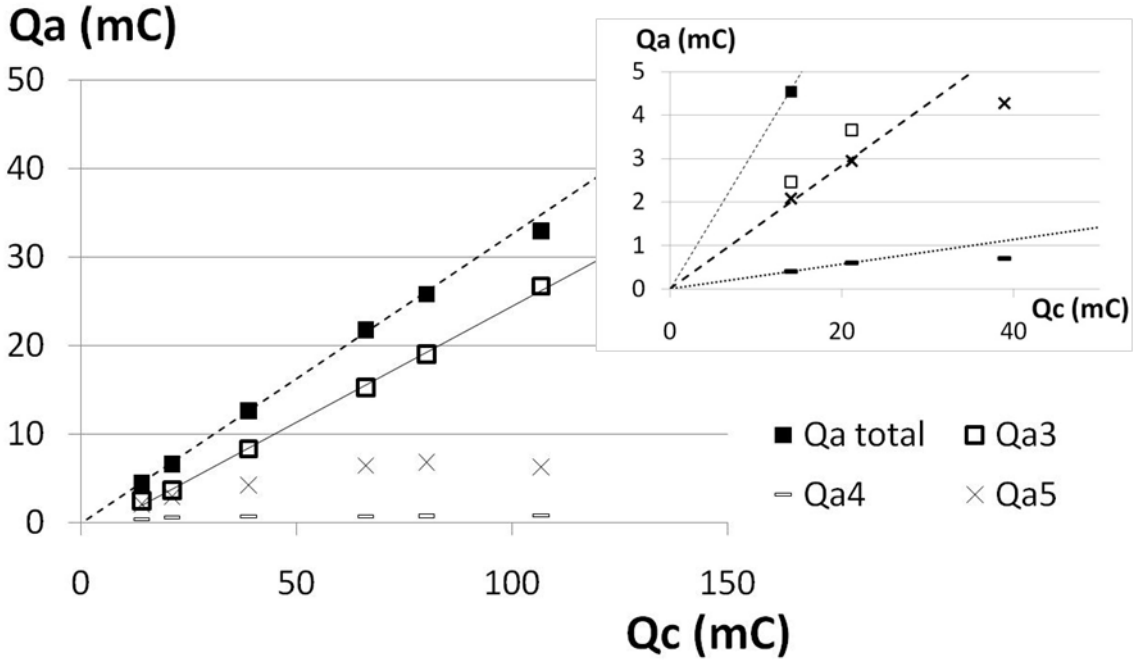

Figure 7

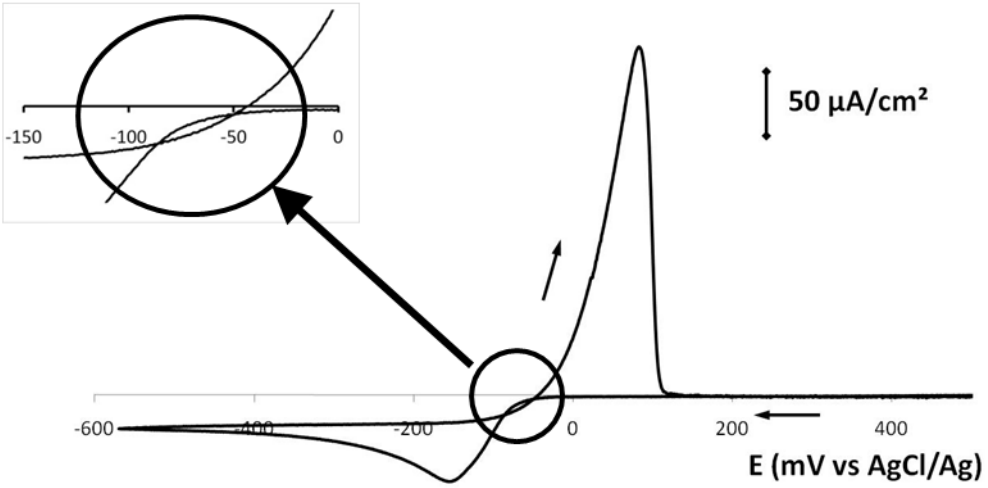

Figure 8

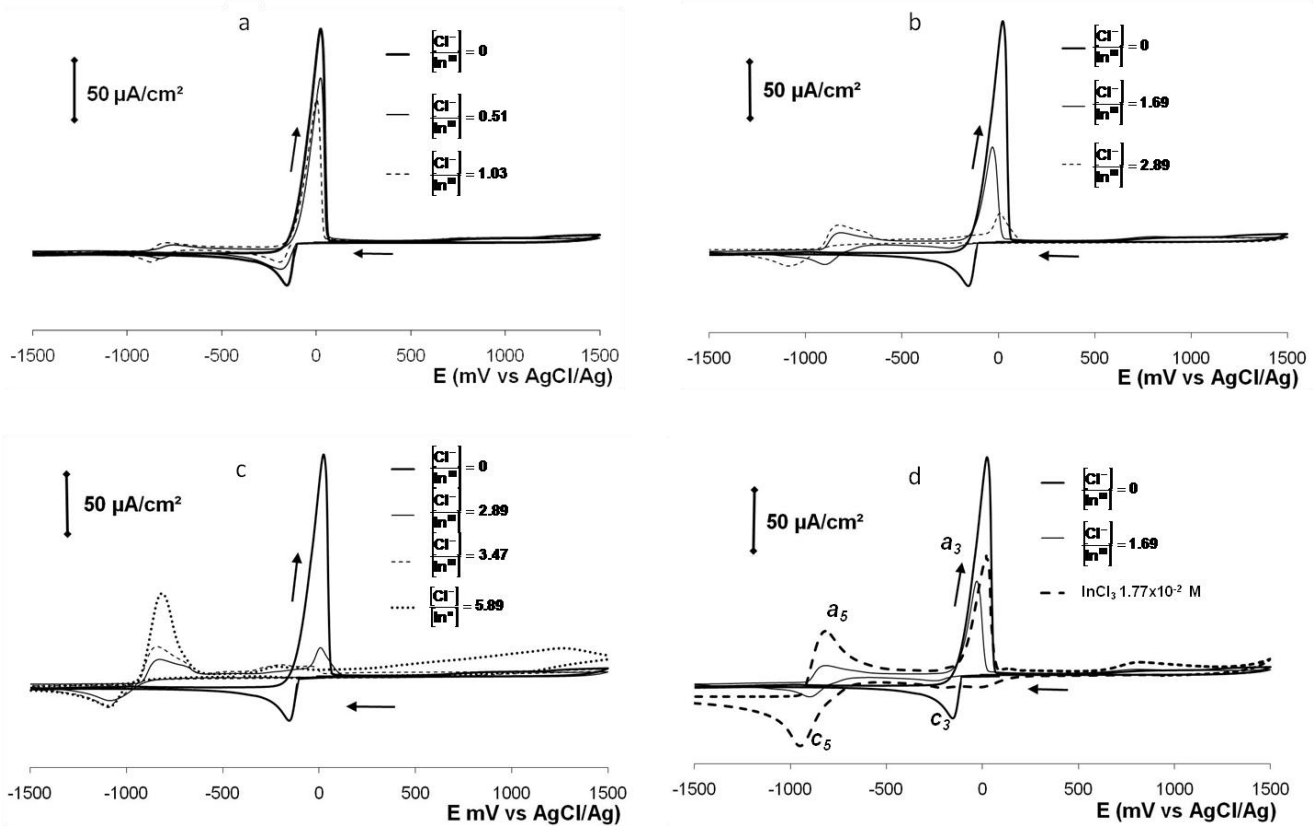

Figure 9

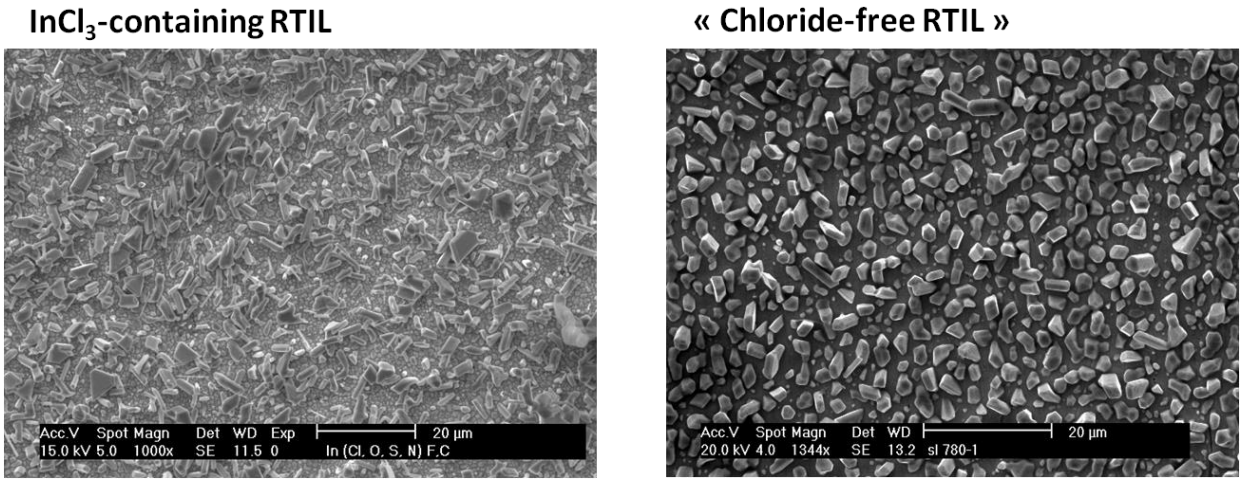

Figure 10

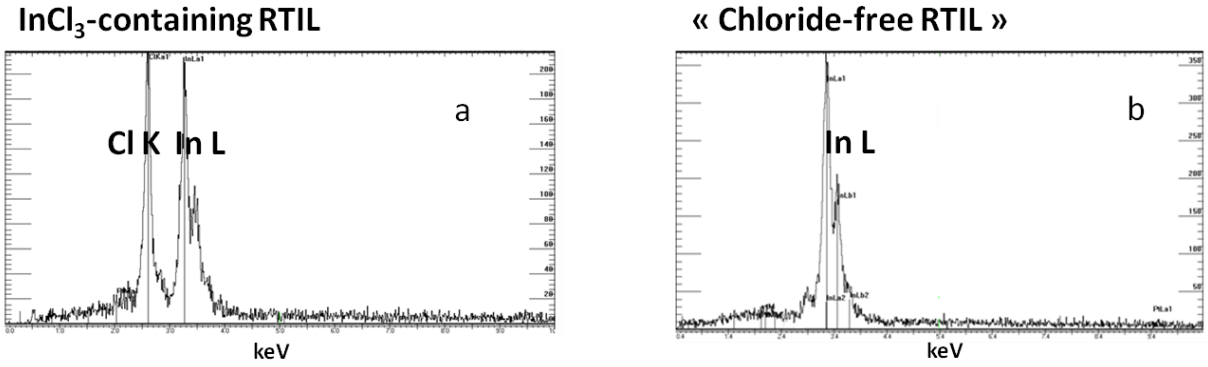

Figures and Tables captions

Table 1: RTILs physicochemical properties

Figure 1: Cyclic voltammograms recorded on platinum in BEPipTf_2N.Scan rate 5 mV/s. T =60°C.

Figure 2: XRD pattern of an indium deposit on a platinum substrate. BEPipTf_2N + $InCl_3$ 0.1 M. E_{dep} = -920 mV vs AgCl/Ag, t_{dep} = 1h. T =60°C.

Figure 3: Cyclic voltammograms recorded in BEPipTf_2N containing 0.1 M $InCl_3$ on platinum and stainless steel. Scan rate 5 mV/s. T =60°C.

Figure 4: Cyclic voltammograms recorded on platinum in BEPipTf_2N containing 0.1 M $InCl_3$ with different reversal potentials. Scan rate 5 mV/s. T =60°C.

Figure 5: Voltammograms recorded during anodic stripping of indium in BEPipTf_2N containing 0.1 M $InCl_3$, for different deposition charge values. Platinum substrate. Scan rate 5 mV/s. T = 60°C. a: E_{dep} = -100 mV vs AgCl/Ag, b: E_{dep} = -200 mV vs AgCl/Ag

Figure 6a: Voltammograms recorded during anodic stripping of indium in $BEPipTf_2N$ containing 0.1 M $InCl_3$, for different deposition charge values. Platinum substrate. Scan rate 5 mV/s. T = 60°C. E_{dep} = -920 mV vs AgCl/Ag.

Figure 6b: Anodic charges corresponding to potentiodynamic stripping of indium *(voltammograms presented in Fig. 6a)* as a function of cathodic charge related to potentiostatic deposition. $BEPipTf_2N$ containing 0.1 M $InCl_3$.Platinum substrate. T = 60°C. E_{dep} = -920 mV vs AgCl/Ag.

Figure 7: Cyclic voltammogram of a 1.87 x 10^{-2} M In(III) solution of chloride-free $BEPipTf_2N$. Scan rate 5 mV/s. T =60°C. Pt substrate.

Figure 8: Cyclic voltammograms of a 1.87 x 10^{-2} M In(III)-containing $BEPipTf_2N$ solution, recorded for different values of the $[Cl^-]/[In(III)]$ ratio. Scan rate 5 mV/s. T =60°C. Pt substrate.

Figure 9: Typical SEM micrographs of indium deposits obtained in $BEPipTf_2N$. Pt substrate. 60 minutes deposition. a: $BEPipTf_2N$ + $InCl_3$ 9.22 x 10^{-2} M. E_{dep} = -920 mV vs AgCl/Ag, b: Chloride-free $BEPipTf_2N$. E_{dep} = -140 mV vs AgCl/Ag. [In(III)] = 7.31 x 10^{-2} M.

Table 2: Electrodeposition of indium on platinum in $BEPipTf_2N$: average faradic yields.

Figure 10: EDS analysis of indium deposits obtained in $BEPipTf_2N$.Pt substrate. 60 minutes deposition. *(Sample presented on Figure 9).* a: $BEPipTf_2N$ + $InCl_3$ 9.22 x 10^{-2} M. E_{dep} = -920 mV vs AgCl/Ag, b: Chloride-free $BEPipTf_2N$. E_{dep} = -140 mV vs AgCl/Ag. [In(III)] = 7.31 x 10^{-2} M.

Tables

Table 1

RTIL Cation	**Density (g/cm^3) 20°C**	**Electro chemical window (V)**	**Cathodic stability (V vs AgCl/Ag)**	**Conductivity (mS/cm) 25°C** *(ppm H_2O)*	**Dynamic viscosity (mPa.s) 20°C** *(ppm H_2O)*	**Kinematic viscosity (mm^2/s) 20°C** *(ppm H_2O)*	**H_2O sat (ppm)**
BMI [a]	1.43918 *(2215)* 1.429 [10]	4.3 3.5 [17]	-1.8	3.3 *(312)* 4.0 [18] 3.9 [10]	58.7 *(2215)* 52 [18]	40.8 *(2215)*	14990
BMP [b]	1.39723 *(537)* 1.41 [10] 1.393 [16]	5.1 4.0 [20]	-2.4	2.6 *(286)* 2.2 [10]	97.8 *(537)* 85 [18] 76 [16]	70.0 *(537)*	13123 11700 [21]
BMPip [c]	1.38342 *(653)* 1.378 [16]	4.8	-2.2	0.93 *(358)* 1.1 [16] 1.3 [21]	248.7 *(653)* 200 [21]	179.8 *(653)* 182 [16]	10115 10050 [21]
MOPip [d]	1.28443 *(781)*	5.1	-2.4	0.40 *(315)*	406.9 *(781)*	316.8 *(781)*	7961 6590 [21]
BEPip [e]	1.36623 *(415)*	4.9	-2.4	0.82 *(150)*	290 *(415)*	212.4 *(415)*	10289
EOPip [f]	1.27426 *(721)*	5.3	-2.5	0.34 *(245)*	423.3 *(721)*	332.2 *(721)*	7157

[a] 1-butyl-3-methyl-imidazolium, [b] 1-butyl-1-methyl-pyrrolidinium, [c] 1-butyl-1-methyl-piperidinium, [d] 1-methyl-1-octyl-piperidinium, [e] 1-butyl-1-ethyl-piperidinium, [f] 1-ethyl-1-octyl-piperidinium

Table 2

Metallic precursor	**E_{dep} (mV vs AgCl/Ag)**	**Yield (%)**
$InCl_3$	-810 ($E_{1/2}$)	33,7
	-920 (E_{peak})	35,6
	-1080	32,2
In anode	-125 ($E_{1/2}$)	65,5
	-140 (E_{peak})	85,5
	-340	77,2

[1] Z.B. Zhou, H. Matsumoto, K. Tatsumi, Chem. Eur. J. 12 (2006) 2196